Experimental and modeling study of acetone combustion

Ismahane Meziane, Yann Fenard, Nicolas Delort, Olivier Herbinet, Jérémy Bourgalais, Ajoy Ramalingam, Karl Alexander Heufer, Frédérique Battin-Leclerc

Experimental and modeling study of acetone combustion

Ismahane Meziane[a], Yann Fenard[b, c*], Nicolas Delort[a], Olivier Herbinet[a], Jérémy Bourgalais [a], Ajoy Ramalingam[c], Karl Alexander Heufer[c], Frédérique Battin-Leclerc[a]

[a] Université de Lorraine, CNRS, LRGP, F-54000 Nancy, France

[b] Univ. Lille, CNRS, UMR 8522 – PC2A, Physicochimie des Processus de Combustion et de l'Atmosphère, F-59000 Lille, France

[c] Chair of High Pressure Gas Dynamics (formerly Physico-Chemical Fundamentals of Combustion), RWTH Aachen University, D-52056 Aachen, Germany

Keywords:

Acetone; Jet-stirred Reactor; Rapid Compression Machine; Pyrolysis; Oxidation; Biomass; Kinetic Modeling; Burning Velocity

*: corresponding author

Abstract

The pyrolysis and oxidation of acetone were studied using three complementary experimental setups. Jet-stirred reactor experiments were performed at four equivalence ratios (ϕ = 0.5, 1, 2, and ∞), at pressure of 1.067 bar (800 Torr) and over the temperature range of 700–1200 K for pyrolysis and 600–1150 K for oxidation. The decomposition of acetone starts around 800 K with a conversion rate of 50% obtained around 1000 K in both pyrolysis and oxidation studies. The main stable products detected in both conditions are small hydrocarbons (methane, ethane, and ethylene), with also acetaldehyde, CO and CO_2 for oxidation. Oscillation behavior was detected beyond 1000 K under oxidation conditions and the products were followed with on-line mass spectrometry. Ignition delay times were measured using a rapid compression machine at pressures of 20 and 40 bar under non-diluted stoichiometric conditions over the temperature range 850-1100 K. The ignition delay times measured in the present study, combined with shock tube data of literature, exhibit a slight inflexion to the Arrhenius behavior, but no negative temperature coefficient. Laminar burning velocities were measured using a flat flame burner at atmospheric pressure for three fresh gas temperatures: ambient temperature, 358 and 398 K. A detailed kinetic model of the combustion of acetone including 852 species and 3265 reactions was developed. This new kinetic mechanism predicts relatively well the experimental measurements of ignition delay times, the mole fraction of the products in the jet-stirred reactor including oscillations and laminar burning velocities. Related flow rate and sensitivity analysis are also presented providing new insights into the acetone reaction network.

1. Introduction

Acetone, CH_3COCH_3, is an important organic solvent used in various industrial processes [1]. Due to its thermodynamic properties (e.g., energy density, heating value, octane number), acetone is considered as an alternative fuel for internal combustion engines and a well-known intermediate in the combustion of hydrocarbons and oxygenates [2–4]. Acetone is a potential solvent in processes proposed to catalytically convert lignin in high-valued fuel commodities [5]. In addition, due to its ability to fluoresce, acetone is commonly used in the laser induced fluorescence (LIF) spectroscopic method as a tracer to map the distribution of fuels in combustion processes [6]. It is an affordable non-toxic tracer whose high vapor pressure (3.06×10^{-1} bar) allows seeding of flows with high concentrations. Its broad absorption feature (225 to 320 nm) is accessible with high-energy pulsed ultraviolet (UV) lasers while fluorescence can be achieved between 350 and 550 nm [6]. Moreover, acetone plays an important role in atmospheric chemistry as the most abundant oxygenated organic species in the upper troposphere [7]. It is produced *in situ* by the oxidation of volatile organic compounds (VOCs) of anthropogenic and biogenic sources [8] and can be emitted by uncontrolled combustion processes [9]. The oxidation of acetone and reactive by-products in the atmosphere promotes the formation of NO_x which are important precursors of tropospheric ozone, a key secondary pollutant [10]. Despite its importance in both industrial processes and atmospheric chemistry, little is yet known about the reactivity of acetone in hot environments and a better understanding of the chemistry of its thermal decomposition and oxidation is needed.

Table 1 summarizes the experimental studies in the literature concerning the oxidation and pyrolysis of acetone. The investigation of the pyrolysis of acetone started in 1974 using flash vaporization [11] in a pyrolysis tube and the formation of CO, methane and H_2 was indicated by

gas chromatography analysis. Later, Ernst et al. [12] used reflected shock waves (1350–1650 K) with time-resolved UV absorption at 290 nm to measure the rate constant of the initiation reaction ($(CH_3)_2CO \rightarrow CH_3CO + CH_3$). Sato and Hidaka [13] used a shock tube to follow the time-resolved evolution of species during acetone pyrolysis (1100–1570 K) by various spectroscopic methods (UV absorption, IR absorption, IR emission) and a single-pulse technique to measure product yields. The main stable products detected were CO, CH_4, C_2H_6, C_2H_4, C_2H_2, and CH_2CO (ketene); C_3H_4 (propyne), C_3H_4 (allene), C_3H_6 (propene), C_3H_8, and 1,3-C_4H_6 were found in lower amounts. In 2018, Yu et al. [14] conducted an experimental and theoretical study on the pyrolysis of acetone in a jet-stirred reactor (JSR). In addition to the species detected by Sato & Hidaka [13], six additional compounds were quantified, namely 1-C_4H_8, iC_4H_8, nC_4H_{10}, iC_4H_{10}, C_5H_6, and C_6H_6. Finally, Zaleski et al. [15] studied the flash pyrolysis of acetone at 1800 K in a heated SiC (Silicon Carbide) micro reactor using broadband rotational spectroscopy. They observed ketene as the major product, together with minor formation of acetaldehyde (CH_3CHO), propyne, and propene. They showed that acetaldehyde directly resulted from the substitution of acetone methyl group by a free H-atom and provided an experimentally derived rate constant at 0.13 mbar and proposed a pressure dependent formulation for this reaction.

Investigations on the gas-phase oxidation of acetone started from 1968 by Barnard and Honeyman [16,17] and Hoare et al. [18,19] using closed Pyrex vessels at temperatures below 800 K. Using the same methods as during their pyrolysis study, Sato and Hidaka [13] also investigated acetone oxidation and published a kinetic mechanism including 164 reactions and involving 51 species. Tsuboi et al. [20] studied the oxidation and decomposition of acetone behind reflected shock waves over the temperature range 1280–1720 K using UV absorption and IR emission. Pichon et al. [21] carried out measurements of acetone ignition delay times behind reflected shock waves over the temperature range 1340–1930 K, at 1 atm and at equivalence ratios of 0.5, 1 and 2. Pichon et al.

[21] developed a kinetic model (81 species and 419 reactions) well predicting ignition delay times (IDTs), as well as their flame velocity measurements described hereafter. As shown in Table 1, to the best of our knowledge, the pyrolysis of acetone has been studied in a JSR [14] but its oxidation has never been studied, neither in a JSR nor in a rapid compression machine (RCM).

Table 1. Summary of the main experimental studies in the literature after 1999 on acetone pyrolysis, oxidation, and flames as well as product mole fraction profiles, IDTs and laminar flame velocities.

Instrument	**Measured property**	**Experimental conditions**			**Reference**
		T **(K)**	***P*** **(bar)**	ϕ	
Shock tube	Ignition delay times	1340-1930	1.013	0.5-1-2	Pichon et al., 2009 [21]
	Mole fraction profiles	1280-1720	0.537-0.790	1	Tsuboi et al., 1999 [20]
		1100-1570	1.216-2.229	∞	Sato and Hidaka., 2000 [13]
		1050-1650	1.216-2.229	0.5-2	
Jet stirred reactor		700-1136	1.013	∞	Yu et al., 2018 [14]
Flat flame burner		273 [a]	2.10^{-2}	1	Li et al., 2008 [22]
		273 [a]	4.10^{-2}	1.5	
		T_{room} [a, b]	2.10^{-2}	0.76	Liao et al., 2021 [23]
		T_{room} [a, b]	4.10^{-2}	1.83	
Constant Volume Chamber	Laminar Burning Velocity	298 [a]	1.013	0.7-1.6	Konnov et al., 2009 [24]
		298-358 [a]	1.013	0.6-1.4	Nilsson et al., 2013 [25]
		298 [a]	1.013	0.8-1.5	Pichon et al, 2009 [21]
		298 [a]	1.013	0.7-1.7	Burluka et al., 2010 [26]
		343, 393 [a]	1.013	0.7-1.6	Gong et al., 2015 [27]
		400 [a]	1.013	0.8-1.6	Zhang et al., 2018 [28]
Stagnation flame burner		298 [a]	1.013	0.75-1.4	Chong et al., 2011 [29]
Bunsen burner		373-523 [a]	1	0.6-1.4	Wu et al., 2016 [30]
		473 [a]	1-10	0.7-1.2	
		433 [a]	1	0.7-1.3	Wu et al., 2017 [31]

[a]Fresh gas temperature, [b]T_{room} is room temperature.

Experiments on flame structure were performed by Li et al. [22] et Liao et al. [23]. Both teams used a flat flame burner at low-pressure and synchrotron vacuum ultraviolet photoionization coupled to molecular beam mass spectrometry (SVUV-MBMS). They observed methyl radical and ketene as major intermediates independent of the mixture composition and methyl-ethyl-ketone and formaldehyde in rich conditions. Additionally, Liao developed a kinetic model including 495 species and 2779 reactions.

Concerning acetone flame velocities, the first measurements were performed using a Bunsen burner from 1959 (Gibbs et al. (1959) [32], Khitrin et al. (1961) [33]); later, as shown in Table 1. Wu et al. [30,31] used this type of burner with chemiluminescence and fluorescence techniques. Laminar flame velocity data were also obtained in constant volume bombs coupled with high speed cameras to record flame propagation by Molkov et al. (1981) [34], and later by Pichon et al. [21], Burluka et al. [26], Gong et al. [27], Zhang et al. [28] and using a stagnation flame burner by Chong et al. [29] with particle image velocimetry. Only the group of Konnov [24] used a flat flame burner combined with the heat flux method. This apparatus presents the advantage of a really low stretch effect ($\approx 1\ s^{-1}$) [35] allowing a direct calculation of the laminar burning velocity from the measured value. On the contrary, most of other methods like the one presented in Table 1, consist in interpolating a value measured with optical systems on a stretched flame what increases uncertainties. The acetone flame velocities under atmospheric pressure and for a fresh gas temperature of 298 K peaked around 35 cm/s at an equivalence ratio (ϕ) of 1.1. However, even without considering the oldest measurements, a significant data scattering is observed with a difference up to 14 cm/s at $\phi = 0.9$. A maximum deviation of 4.5 cm/s at 298 K was observed between the two studies performed using both the heat flux method. Very few data, only three measurements at 358 K ($\phi = 0.6$, 0.7 and 1) using the heat flux method, were obtained for higher

fresh gas temperatures, and here also with a significant dispersion of the data. New kinetic models were proposed by Pichon et al. [21] (mentioned before), Burluka et al. [26] (129 species and 1252 reactions) and by Zhang et al. [28] (247 species and 1378 reactions); Chong et al. [29] and Nilsson et al. [25] only updated respectively Pichon et al.'s and Burluka et al.'s models.

In conclusion of the previous concise literature review, the aim of the present work is to perform experimental measurements in:

- a JSR (Nancy) over a temperature range from 600 to 1200 K (pressure of 106.7 kPa and residence time of 2 s) under oxidative and pyrolytic conditions with product quantification,
- a RCM (Aachen) at pressures of 20 and 40 bar under non-diluted stoichiometric conditions over the temperature range 850-1100 K with IDT recording,
- a flat flame burner (Nancy) to measure laminar flame velocities (heat-flux method) at atmospheric pressure, and three temperatures: ambient, 358, and 398 K.

The obtained results are then used to develop and validate a kinetic model of acetone pyrolysis and oxidation.

2. Experimental methods

This section describes the used experimental techniques, i.e. the JSR set-up and the connected analytical procedures, the RCM device, and the flat flame burner (see experimental conditions in Table S1-S3 in supplementary material (SM)), as well as the numerical methods enabling to simulate these experiments. Since the three experimental devices used have already been described in detail in the literature, only a brief description is provided here. The reactants used in Nancy were oxygen (purity ≥ 99.999%), helium (purity ≥ 99.999%), and nitrogen (purity: 99.995%) provided by Messer France, and acetone (purity ≥ 99.8%) by Carlo Erba Reagents. In Aachen, both the oxygen and the nitrogen are of ≥ 99.999% purity and were obtained from Westfalen AG and

argon (purity ≥ 99.996%) from Linde AG. Acetone was supplied by Sigma-Aldrich was of HPLC grade ≥ 99.9%.

2.1 JSR experiments

2.1.a. JSR set-up

The JSR setup at LRGP-Nancy has been frequently used in the studies of thermal decomposition and oxidation of hydrocarbons (e.g. Herbinet et al. [36]), oxygenated (e.g. Namysl et al. [37]) and nitrogenized (e.g. Pelucchi et al. [38]) liquid fuels. The reactor consists of a 92 cm^3 fused silica sphere, into which the gases enter through a centrally located injection cross, which is composed of four nozzles providing turbulent jets for an efficient mixing. The heating of the reactor is achieved through Thermocoax heating elements fitting the spherical shape of the JSR. The temperature is controlled by Eurotherm 3216 controllers and K-type thermocouples. To ensure a homogeneous temperature in the JSR, the fresh gas mixture is preheated and diluted in an inert gas to avoid significant temperature gradients due to the oxidation exothermicity. The pressure is regulated by a valve downstream of the reactor. Calibrated mass and Coriolis flow controllers are used to control gas and liquid flow rates and the liquid fuel is mixed homogeneously into the gas flow using He as a carrier gas through a controlled evaporation mixing system (CEM, Bronkhorst). The relative uncertainty in liquid and gas flow rates is about 0.5%.

The acetone pyrolysis and oxidation experiments were performed at a constant pressure of 1.067 bar, a residence time of 2 s, for three equivalence ratios (0.5, 1, and 2), for an initial fuel mole fraction of 0.01, and over the temperature range 700–1200 K for pyrolysis and 600-1150 K for oxidation. Simulations were performed using the perfectly stirred reactor (PSR) module in the Chemkin software [39].

2.1.b. Gas chromatography analyses

The products leaving the JSR are transported through a heated (T = 353 K) transfer line for analysis using three GCs. A first gas chromatograph, equipped with a Carbosphere packed column and a thermal conductivity detector (TCD), is used for the quantification of light-weight compounds, such as oxygen, methane, carbon monoxide and carbon dioxide. The identification of C_{2+} species is performed using a second GC, which is fitted with a Q-Bond capillary column and coupled to a mass spectrometer with a standard 70 eV electron ionization. A third GC, fitted with a Q-Bond capillary column and a flame ionization detector (FID) preceded by a methanizer, is used for the quantification of compounds containing from 1 carbon atom, e.g., CO, CO_2, methane, up to compounds with 6 carbon atoms, e.g., benzene. Due to their complete hydrogenation, the methanizer (nickel catalyst) allows the diagnostic to be sensitive to the detection of carbonyl-bearing species like CO and CH_3CHO. FID and TCD calibrations are performed using gaseous standards provided by Air Liquide for O_2, CH_4, CO, and CO_2. The other species detected with the FID are calibrated using the effective carbon number (ECN) method. The relative uncertainties of the mole fractions of the species detected by GC and calibrated using gaseous standards were estimated to be ±5% [40] while the relative uncertainties of the mole fractions of the species calibrated using the ECN method were estimated to be ±10%. A good reproducibility between TCD and FID measurements allowing the quantification of similar species (CO, CO_2, and CH_4) was observed (see results here-after). As shown in Table S4 in SM, the carbon atom balance is above 90%, except between 975 and 1100 K under pyrolysis condition, when it drops down to 82% at 1050 K.

2.1.c. Product analysis during oscillation behavior in JSR experiments

Oscillation behavior (periodic transient variations of mole fraction as a function of time) was observed with acetone beyond 1000 K under oxidation conditions. This transient evolution of temperature and of mole fractions of reactants and products have already been reported during oscillating limit cycles during JSR fuel oxidation [41]. In order to measure the evolution of species mole fraction during these oscillations, a quadrupole mass spectrometer (MS) with in-line sampling was used. The sampling line consisted of a capillary tube with a fused silica portion connected to the JSR and a stainless-steel portion connected to the MS. Signal at *m/z* 58, 44, 32, 28, 16 and 2 were recorded and were attributed to acetone, carbon dioxide, oxygen, carbon monoxide, methane, and hydrogen, respectively. A direct calibration was performed for the fuel and oxygen. For reaction products, the calibration was performed using mole fractions obtained from gas chromatography under non-oscillating conditions as reference. Relative uncertainties in mole fractions are ±10% for the fuel and oxygen, and ±20% for reaction products.

2.1. RCM experiments

Previous descriptions of the high-pressure RCM at HGD, RWTH Aachen University can be found in Lee et al. and Ramalingam et al. [42,43]. The heating of the mixing vessels, manifold, and the reaction chamber is controlled and monitored by type T thermocouples. The mixture is prepared by monitoring the partial pressures with the help of two static pressure sensors (STS ATM.1ST: 0−0.5 bar, STS ATM.1ST: 0−5 bar). The pressure change in the reaction chamber is recorded with a Kistler 6125C11U20 pressure sensor. The compressed temperature is calculated with the aid of the adiabatic compression and expansion routine of Gaseq [44]. The contributing factors to the IDT measurement uncertainties have been discussed in Ramalingam et al. [43], and therefore, only the evaluated values are listed. The compressed temperature uncertainty is estimated to be within ±5

K, and the IDT variation is within 20%. Non-reactive pressure profiles are obtained for each measured temperature point to account for the facility effects during simulations. The simulation method for IDT has been discussed and outlined in the review works [45,46]. In brief, the initial conditions of pressure, temperature, mixture composition, and the selected mechanism along with the converted effective volume time histories obtained from the non-reactive pressure profiles are used as inputs for the zero-dimensional simulation of the IDT. Figure 1 shows the IDT measurement for acetone at 20 bar under stoichiometric condition along with its non-reactive and simulated pressure trace.

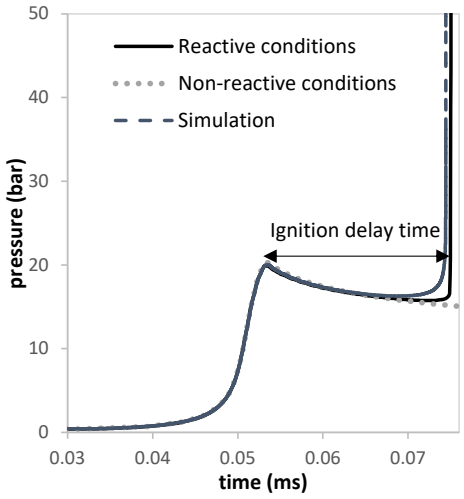

Fig. 1. Pressure traces of non-diluted stoichiometric acetone mixtures at 20 bar.

2.2. Flame experiments

The flat-flame burner in LRGP-Nancy was built following the design established by De Goey [35] and has been used previously to measure the laminar flame velocities of gasoline components including ethanol [47] and oxygenated biofuels such as tetrahydrofuran [48]. The burner head is a circular perforated brass plate of 30 mm diameter and 2 mm thickness. Holes are 0.5 mm diameter and are spaced by a pitch of 0.7 mm. Eight type K-thermocouples of 0.5 mm diameter are soldered

in the plate from the center to the periphery at different angles. This plate is mounted on a plenum chamber surrounded by a heating jacket to control fresh gas temperature. The exit plate is also heated by another heating system, from its periphery, to ensure adiabatic conditions. During combustion, heat loss occurs from the flame to the burner, so the plate is heated (about 50 K higher fresh gas) to bring heat flux to unburnt gas and compensate energy loss. If the fresh gas velocity is lower (respectively higher) than the adiabatic burning velocity, heat losses are higher (respectively lower) than the input energy. The flame is thus stabilized under subadiabatic (respectively superadiabatic) conditions, which implies a higher (respectively lower) temperature at the center of the plate measured by thermocouples. Under adiabatic conditions, heat losses and gain balance out and a flat temperature profile is observed on the burner plate. In this case, it has been shown that the velocity of the adiabatic flame is equal to the velocity of the gas.

Oxygen and nitrogen flow rates are regulated by Bronkhorst High-Tech Mass Flow Controllers and the liquid fuel flow rate is monitored using a Bronkhorst mini-CORI-FLOW Mass Flow Controller. The fuel, stored in a tank, is mixed to nitrogen before entering an evaporator. This mixture is then blended to oxygen to redial an artificial air (21% O_2 + 79% N_2) before being injected in the plenum chamber.

The uncertainties of the laminar flame velocity measurements vary with the experimental conditions (fuel, T, P, ϕ) and thus calculated for each case. The uncertainties of the mass flow controllers are 0.2% plus an error of 0.5 g/h, 0.8%, and 0.2% for fuel, oxygen, and nitrogen respectively. This leads to a global maximum error on laminar flame velocity of 0.55%. A maximum error on laminar flame velocity of 1.92% due to the flat temperature profile is estimated. A maximum uncertainty of 2.1% is due to the temperature in the plenum chamber. Finally, an error of 0.2 cm/s is attributed to other sources of uncertainty that are difficult to quantify (e.g., flame

distortion, like edge effects, purity of compounds). This leads to a maximum relative uncertainty of 8.6 % and a maximum absolute uncertainty of 1.41 cm/s on burning velocity. The equivalence ratio error due to uncertainties of the fuel and oxygen mass flow controllers is estimated to 1%.

3. Kinetic modeling

A new kinetic model has been developed in this work and is provided as SM in CHEMKIN format with thermochemical and transport data. A nomenclature is also given in Table S5 in SM. Because AramcoMech 3.0 has been widely chosen as base mechanism for large molecules and shows superior performance, it is the base mechanism in this work [49]. It is part of the development of a common model for C_3-C_5 ketones whose details can be found for 2- and 3-pentanone [50]. The reaction classes considered are similar to alkanes [51]. Reactions arising from interactions between the acetonyl radical and molecular oxygen are included for completeness. The thermal decomposition of acetone giving methyl and acetyl radicals is analogous to butanone [52], however increased by a factor of 4 compared to butanone and 2-pentanone to consider the influence of the higher pressure dependence of small species in unimolecular reactions. Saxena et al. [53] calculated this reaction rate constant with variable reaction coordinate transition state theory (VRC-TST). According to [54], a factor of 2 of uncertainty on the reaction rate constant is expected with this method. Furthermore, the authors mention an additional 30% uncertainty due to the fitting with Troe parameters for pressure dependency. This computational method also provides an uncertainty on the barrier energy of the transition state as well as CCSD(T)/sugh-cc-pVTZ+2df//MP2(full)/6-311++G(2d,2p) [55], CBS-QB3 [57] or G3//MP2/aug-cc-pVDZ level of theory [52]. It can be estimated as 1 kcal/mol uncertainty on the activation energy which leads to a factor of 1.65 deviation on the reaction rate constant at 1000 K. With these considerations, multiplying the reaction rate constant from Thion et al. [52] by 4 ends up with a factor of 3 higher than the

calculation by Saxena et al. [53], within the uncertainty of their calculations and fittings. This reaction rate constant is in good agreement with recent works on acetone combustion kinetics as shown in Figure 2.

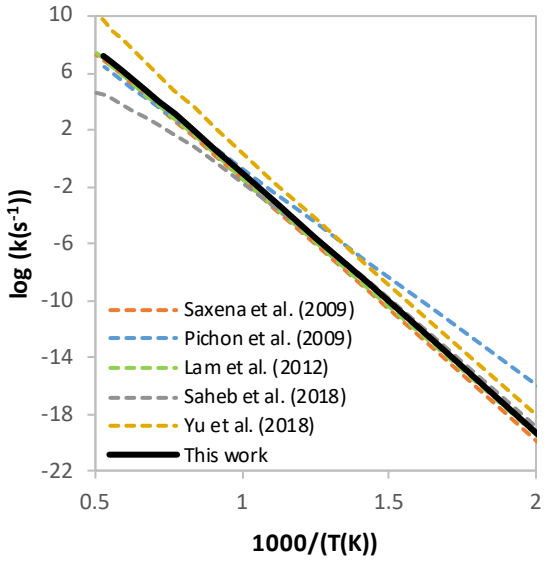

Fig. 2. High pressure limit reaction rate constants for the thermal decomposition of acetone CH_3COCH_3=CH_3CO+CH_3. Comparison of this work with Pichon et al. [21]*, Saxena et al.* [53]*, Saheb et al.* [55]*, Lam et al.* [56] *and Yu et al.* [57].

The H-atom abstraction reactions from the fuel by OH and HO_2 were calculated by Zhou et al. [58] and Mendes et al. [59], respectively. The activation energy for H-atom abstraction by HO_2 was decreased by 3 kcal/mole for optimal performance, as suggested by Fenard et al. and Thion et al. [50,52]. All other rate coefficients are derived from a 2-pentanone kinetic modeling work, [50] which mainly consists of analogies with butanone. In case reaction rate parameters cannot be found for ketones, adapted ones from alkanes are used. Table 2 details the origin of the data used.

Table 2: Acetone detailed kinetic reaction sub-mechanism used in the present study ($k = A \times T^n \times exp\ (-\frac{E_a}{RT})$) in units of s, cm^3, mole, calories.

N°	Reaction	A	n	E_a	Ref.
1	CH_3COCH_3(+M)<=>CH_3+CH_3CO(+M)	2.689E+28	-3.360	88546.3	[52][a,b,c]

2	$CH_3COCH_3(+M)<=>CH_3COCH_2+H(+M)$	6.108E+16	-0.275	97579.1	[52][a,c]
3	$CH_3COCH_3+O2<=>CH_3COCH_2+HO_2$	4.100E+13	0.000	49150.0	[52][a]
4	$CH_3COCH_3+OH<=>CH_3COCH_2+H_2O$	1.326E+02	3.290	-1001.4	[58]
5	$CH_3COCH_3+HO_2<=>CH_3COCH_2+H_2O_2$	3.972E-03	4.510	13635.1	[59][d]
6	$CH_3COCH_3+H<=>CH_3COCH_2+H_2$	1.476E+05	2.877	7093.0	[60][a]
7	$CH_3COCH_3+CH_3<=>CH_3COCH_2+CH_4$	1.733E+00	3.892	8229.0	[60][a]
8	$CH_3COCH_3+O<=>CH_3COCH_2+OH$	1.000E+13	0.000	5962.0	[52][a]
9	$CH_3COCH_3+CH_3O<=>CH_3COCH_2+CH_3OH$	4.340E+11	0.000	4660.0	[52][a]
10	$CH_3COCH_3+C_2H_3<=>CH_3COCH_2+C_2H_4$	1.230E+11	0.000	4278.0	[52][a]
11	$CH_3COCH_3+C_2H_5<=>CH_3COCH_2+C_2H_6$	1.000E+11	0.000	11600.0	[52][a]
11	$CH_3COCH_3+CH_3O_2<=>CH_3COCH_2+CH_3O_2H$	4.460E-05	5.091	12422.7	[61]
12	$CH_3COCH_3+CH_3COCH_2O_2<=>CH_3COCH_2+C_3KET21$	4.460E-05	5.091	12422.7	[61]
13	$CH_3COCH_3+H<=>CH_3CHO+CH_3$	7.096E+12	-0.076	7920.7	[52][a]
14	$CH_3COCH_2<=>CH_3+CH_2CO$ duplicate	4.190E+18	-1.600	38408.5	[52][a,c]
15	$CH_3COCH_2<=>CH_3+CH_2CO$ duplicate	1.083E+15	-0.503	61517.2	[52][a,c]
16	$CH_3COCH_2+ H<=>CH_3CO+CH_3$	1.214E+53	-10.445	44763.9	[52][a,c]
17	$CH_3COCH_2+O_2<=>CH_3COCHO+OH$	1.050E+04	1.800	40324.0	[61][c]
18	$CH_3COCH_2+O_2<=>CH_2COCH_2O_2H$	1.310E-04	3.770	23378.0	[61][c]
19	$CH_3COCH_2+O_2<=>CH_3COCH_2O_2$	2.000E+13	-0.640	29.0	[61][c]
20	$CH_3COCH_2O_2<=>CH_3COCHO+OH$	7.810E+06	1.310	62005.0	[61][c]
21	$CH_3COCH_2O_2<=>CH_2COCH_2O_2H$	1.020E+03	2.200	47829.0	[61][c]
22	$CH_2COCH_2O_2H=>CH_2O+OH+CH_2CO$	4.190E+18	-1.600	38408.5	[52][a,c]
23	$CH_2COCH_2O_2H<=>CYC_3KET_2+OH$	6.767E+09	0.460	17700.0	[62][f]
24	$CH_2COCH_2O_2H+O_2<=>O_2CH_2COCH_2O_2H$	1.000E+13	-0.640	29.0	[61][g]
25	$O_2CH_2COCH_2O_2H<=>HCOCOCH_2O_2H+OH$	1.020E+03	2.200	45829.0	[62][h]
26	$HCOCOCH_2O_2H=>CH_2O+HCO+CO+OH$	1.802E+41	-7.826	55289.5	[52][a,c]
27	$CH_3COCH_2+HO_2<=>CH_3COCH_2O+OH$	8.168E+25	-3.620	14669.2	[52][a,c]
28	$CH_3COCH_2+CH_3COCH_2O_2<=>CH_3COCH_2O+CH_3COCH_2O$	5.080E+12	0.000	-1411.0	[63]
29	$CH_3COCH_2+CH_3O_2<=>CH_3COCH_2O+CH_3O$	8.168E+25	-3.620	14669.2	[52][a]
30	$C_3KET21+O_2<=>CH_3COCH_2O_2+HO_2$	3.746E+13	-0.791	33620.0	[62]
31	$CH_3COCH_2O_2+CH_3COCH_2O_2=>CH_3COCH_2O+CH_3COCH_2O+O2$	1.400E+16	-1.610	1860.0	[62]
32	$CH_3COCH_2O<=>CH_3CO+CH_2O$	5.730E+13	-0.025	4473.5	[52]

[a]: analogy to butanone. [b]: pre-exponential factor enhanced by a factor of 4 compared to butanone. [c]: high pressure limit. [d]: activation energy decreased by 3 kcal/mol. [f] : pre-exponential factor reduced by a factor of 3 [50]. *[g]: second addition to O_2 similar to first addition to O_2 divided by 2* [62]. *[h]: analogy with alkane* [62] *with a reduction of E_a by 2 kcal/mol*

The sub-mechanism of acetone also contains the chemistry of butanone and methyl vinyl ketone to ensure the accuracy of the model as the reaction of acetonyl + methyl radical leads to the formation of butanone, which can yield methyl vinyl ketone. The validation of the butanone and methylvinyl ketone on IDTs available in the literature [45,64–66] are presented in SM. The thermodynamic properties of acetone (CH_3COCH_3), acetonyl (CH_3COCH_2), acetonylperoxy radical

($CH_3COCH_2O_2$) and oxyacetonyl (CH_3COCH_2O) were calculated with methods described in [50]. The thermodynamic data for other species in the acetone submechanism were estimated via group additivity methods [68]. The transportation data were taken from RMG [68].

4. Results and discussion

The JSR pyrolysis of acetone is discussed first. Then the measurements concerning the oxidation of acetone both in RCM and JSR are described. Finally, the data obtained for laminar flame velocities are presented. All the experimental measurements are provided in spreadsheets provided in SM. The data obtained experimentally are compared with the predictions using the kinetic model described in the previous section.

4.1. Thermal decomposition of acetone

The JSR pyrolysis experiments were performed over the temperature range 700-1200 K, with a residence time of 2 s and a pressure of 1.067 bar. As is shown in Figure 3, the major products quantified are carbon monoxide (CO), methane (CH_4), ethylene (C_2H_4) and ethane (C_2H_6), in agreement with the study of Yu et al. [14]. Propyne (C_3H_4), allene (C_3H_4), propene (C_3H_6), 1,3-butadiene (C_4H_6), 1-butene (C_4H_8), acetaldehyde (C_2H_4O) and benzene (C_6H_6) were found as minor species.

Figure 3a shows the mole fraction profile of acetone, whose decomposition starts around 875 K, with a conversion of 50% obtained around 1000 K. Above 1175 K, acetone conversion is complete. The acetone mole fraction profile is well reproduced by the kinetic model. This is also the case for the mole fractions of CO Figure 3b, one of the three products produced in largest amounts. The mole fraction of CH_4 (Figure 3c) and C_2H_4 (Figure 3d), the two other major products, are also well predicted.

The experimental mole fraction profile of propyne (Figure 3f), allene (Figure 3g), propene (Figure 3h), and benzene (Figure 3i) is well captured by the kinetic model. Under pyrolysis conditions, the benzene formation can be explained by the recombination of propargyl radicals as investigated by Miller et al. [69]. At 1100 K, the peak mole fraction of C_2H_6 (Figure 3e) and C_3H_6 (Figure 3h) are underpredicted by 38% and 21% respectively; higher deviations are observed for C_4 products and acetaldehyde.

As shown in Figure SM1, the inclusion of the reaction between acetone and atomic hydrogen forming acetaldehyde ($CH_3COCH_3+H<=>CH_3CHO+CH_3$) with a rate coefficient of 8.745×10^7 s^{-1} as proposed by Zaleski et al. [15] leads to the same prediction of the mole fraction for the major products using the present kinetic model. Acetaldehyde is however more overestimated than with the unmodified kinetic model over the temperature range 1000-1125 K.

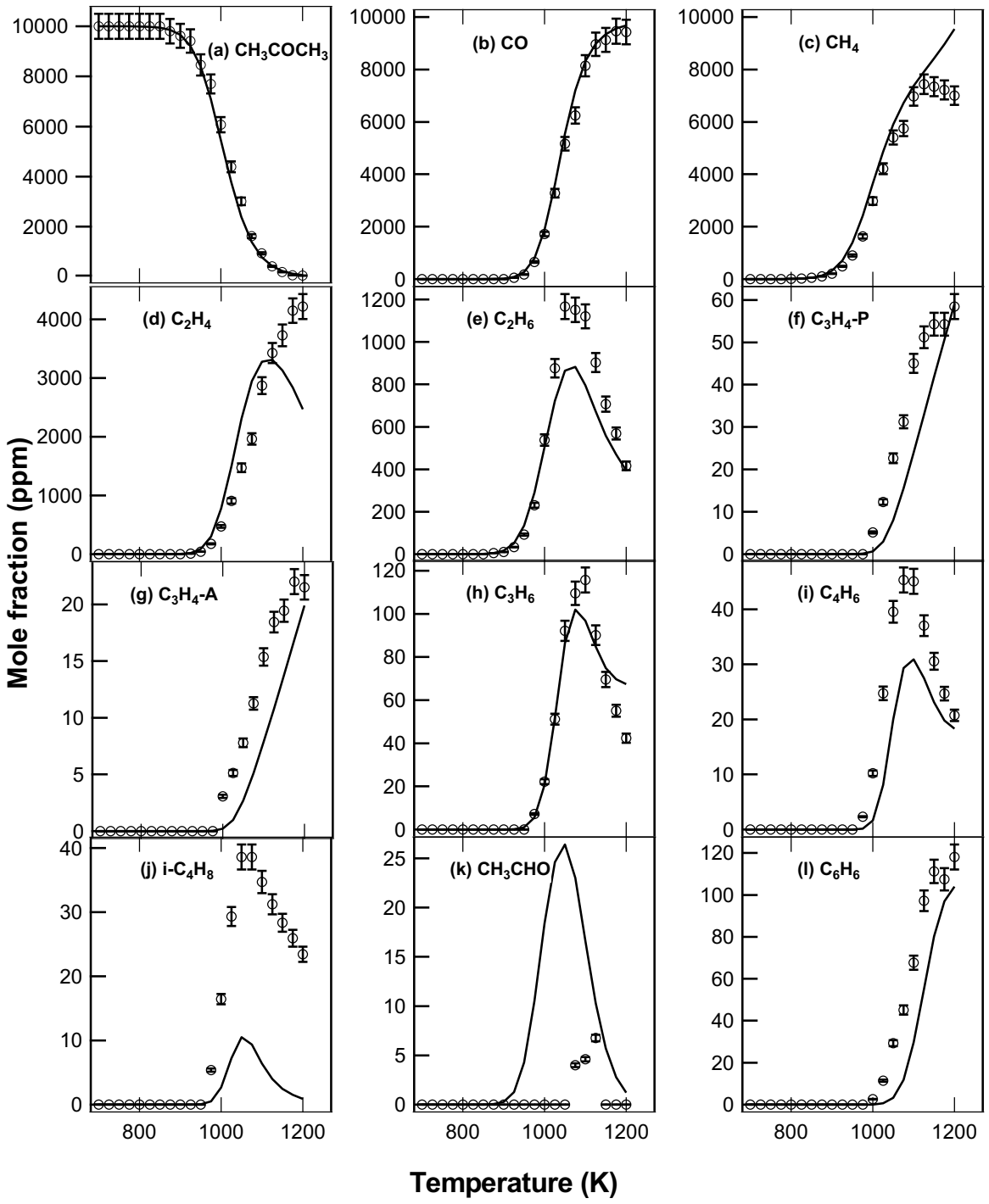

Fig. 3. Mole fraction profiles of acetone and products during the pyrolysis of acetone in a JSR at P = 1.067 bar and τ = 2.0 s. Symbols: experimental data; and lines: computed data.

A flow rate analysis for acetone consumption and a sensitivity analysis on the acetone mole fraction were performed at 1000 K where 50% of acetone is consumed (Figure 4 and Figure 5, respectively). Acetone is converted through two main reaction pathways. The major route of acetone consumption (70.3% of the flux) at pyrolysis conditions is the H-atom abstraction by methyl radicals (R7 of Table 2), which produces methane and a CH_3COCH_2 radical. CH_3COCH_2 undergoes a β-scission reaction forming ketene (CH_2CO), a stable product for which the GC is not sensitive. Ketene reacts through methyl addition followed by a fast decomposition giving carbon monoxide and an ethyl radical. This latter intermediate leads to ethylene. Ethylene leads to the formation of acetylene by H-abstraction and of propene by addition of methyl radical. Acetylene is the source of propyne, then allene and benzene.

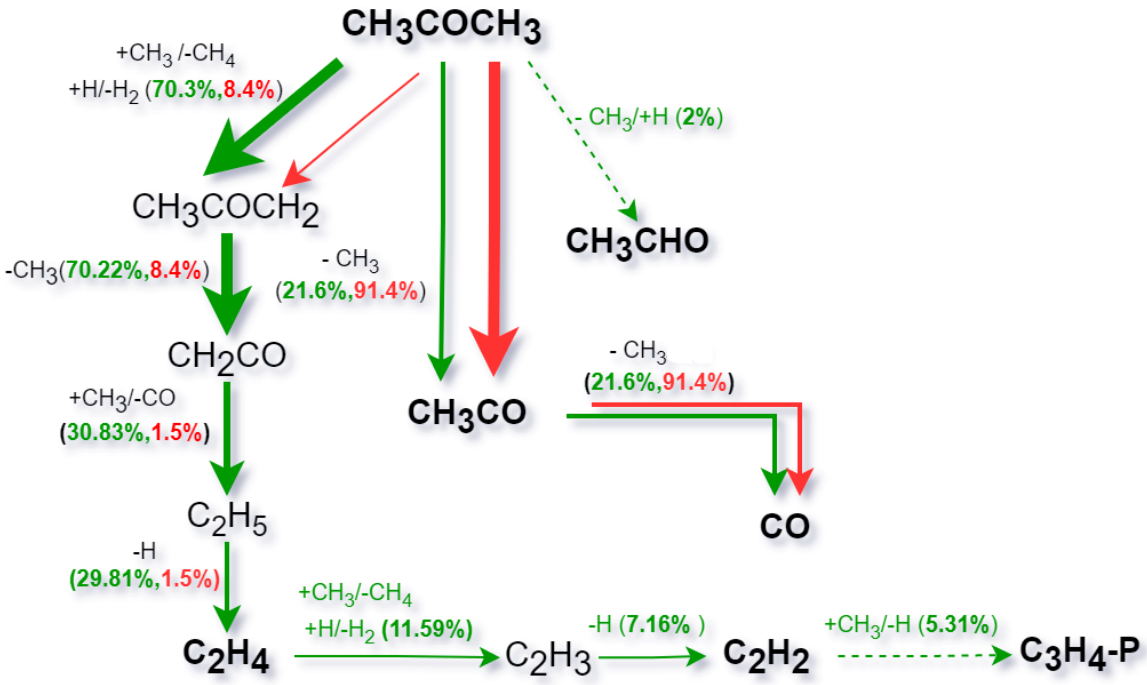

Fig. 4. Rate of consumption analysis for acetone pyrolysis at 1000 and 1200 K (1.067 bar, residence time of 2 s). The size of the arrows is proportional to the reaction flow of acetone consumption as indicated by the numbers in parenthesis (green color for 1000 K, red color for 1200 K).

The second consumption pathway (21.6% of the flux) is acetone unimolecular decomposition (R1) leading to methyl and acetyl radicals (CH_3CO), which decomposes completely to produce CO and again a methyl radical. Methyl radicals essentially recombine together to produce ethane or react with the fuel to yield methane. A minor route of acetone consumption (<2% of the flux) is the addition of a H-atom followed by a CH_3-elimination to produce acetaldehyde, a minor product. The over-estimation of acetaldehyde by the kinetic model might be due to uncertainties in the kinetic parameters of this minor pathway forming acetaldehyde directly from the fuel. When temperature increases, the acetone unimolecular decomposition starts to be dominant (this channel account for 90% of acetone consumption at 1200 K) and the H-abstraction pathway is of lower importance. This explains why the model predicts C_2H_4 mole fraction decreases when the CH_4 mole fraction increases.

A second flow rate analysis was performed at 1200 K where about 100% of acetone is consumed indicating that the main channel consuming acetone (91.4% of the flux) is the unimolecular decomposition (R1) leading to methyl and acetyl radicals (CH_3CO).

The sensitivity analysis on the mole fraction of acetone is performed at 1000 K under the conditions of Figure 4. It confirms that the unimolecular decomposition of acetone (R1) and its H-atom abstraction by methyl radical (R7) have the highest promoting effect on acetone consumption. Since it competes with reaction R7, the recombination of two CH_3 radicals has the strongest inhibiting effect for acetone consumption.

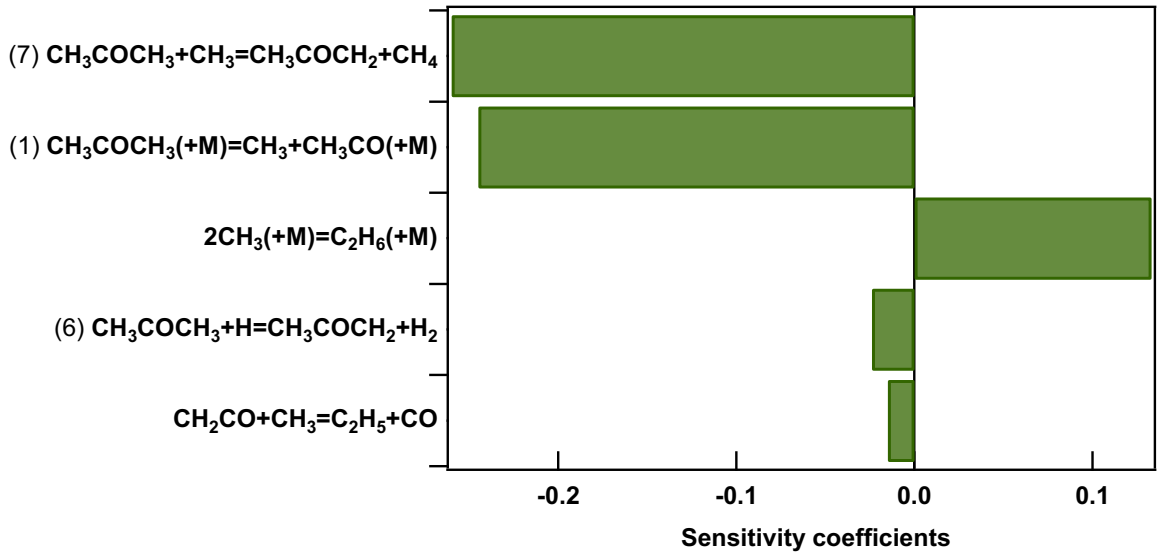

Fig. 5. Sensitive reactions to the mole fraction of acetone during pyrolysis at 1000K and corresponding to 50 % of conversion (first-order local sensitivity coefficients are: $S_{i,j} = \partial \ln(\text{mole fraction of i}) / \partial \ln(\text{reaction rate of j})$). Only reactions, for which the absolute value of the sensitivity coefficient is above 0.02 are shown.

4.2. Oxidation of acetone

This section displays the experimental data obtained with the RCM and the JSR under oxidation conditions. The last part presents the adiabatic laminar burning velocity measurements. All these data are compared with the predictions using the kinetic model developed in the present work. The specificities of the acetone gas phase chemistry are highlighted through kinetic analyses.

4.2.1. Ignition delay times

Figure 6 displays the ignition delay times of acetone measured at pressures of 20 and 40 bar under non-diluted stoichiometric conditions over the temperature range 850-1400 K. The experimental IDTs exhibit an apparent Arrhenius behavior but a change in reactivity is visible at lower temperatures.

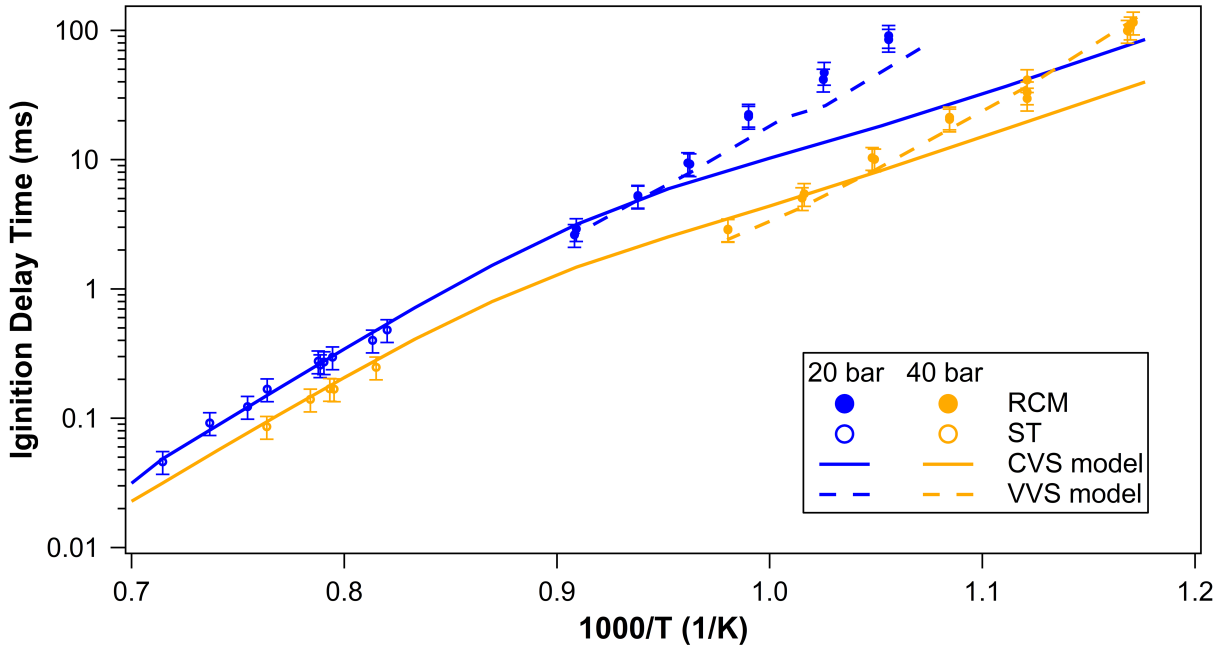

Fig. 6. IDTs of non-diluted stoichiometric acetone/O_2/inert mixture in a RCM (circles) and in a shock tube (squares) at 20 bar (open symbols) and 40 bar (full symbols). Simulations: single lines constant volume simulations, double lines: variable volume simulations.

To get a deeper insight into the auto-ignition mechanism of acetone, sensitivity analysis on IDT were performed in two temperature regimes. A negative coefficient indicates that the reaction contributes to a decrease in IDT and therefore to an increase in reactivity as to the reverse one positive coefficient indicates a reaction that decreases reactivity. At higher temperatures, the unimolecular decomposition of acetone dominates the reactivity as depicted in Figure 7. This reaction strongly enhances the reactivity as it enhances the fuel conversion. On the contrary, the H-atom abstraction reaction by H-atom inhibits the reactivity. Interestingly, the H-atom abstraction reaction from acetone by OH inhibits the reactivity at higher temperatures but promotes the reactivity at 900 K. At this temperature, the unimolecular decomposition of acetone forming CH_3 is slow and does not compete with the H-atom abstraction reactions. Under intermediate temperatures, the fastest steps to produce the reactivity enhancer that is methyl radical is the

production of acetonyl radicals. The fastest reaction to CH_3COCH_2 is acetone + OH. At T = 1400 K, the radical pool is mainly populated with methyl radicals produced via unimolecular decomposition of acetone and by acetone + CH_3 giving CH_4, CH_3 and ketene in a two-step pathway.

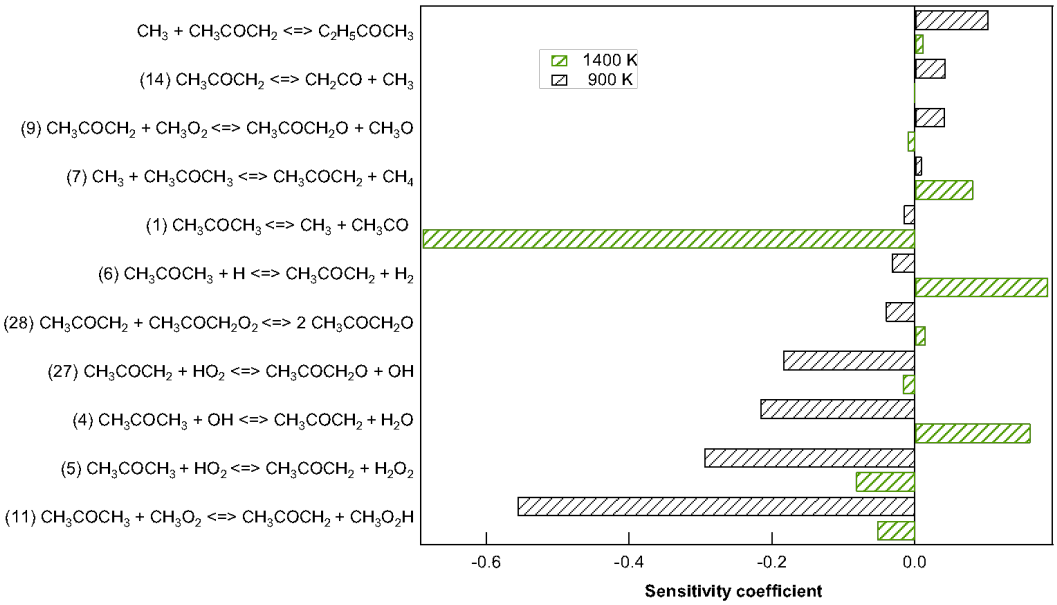

Fig. 7. Sensitivity analysis on the acetone specific reactions on IDTs of non-diluted stoichiometric acetone/O_2/inert mixtures at 40 bar at 900 and 1300 K. Sensitivity coefficient are: $\sigma_i = \log(\tau_i^+/\tau_i^-)/ (\log (2.0/0.5))$ where τ_i^+ is the IDT calculated with an increase of a factor of 2 in the reaction i (k_i), and τ_i^- is the IDT calculated with a decrease of a factor of 2 per k_i.

The examination of the constant volume simulations unravels a deviation from Arrhenius behavior that can be attributed to the low temperature chemistry of combustion. At 900 K, the species controlling the reactivity are peroxyl radicals [70]. The acetonyl radical can add to molecular oxygen to form a peroxylacetonyl radical (RO_2). The short carbon chain of acetone hinders the intramolecular H-atom migration reaction of peroxylacetonyl giving hydroperoxylacetonyl radical. As a consequence, a pathway consuming RO_2 is its reaction with an acetonyl radical yielding two acetonyloxy radicals which formation enhances the reactivity. However, the H-atom abstraction reactions from acetone by HO_2 and CH_3O_2 radicals, enhance the reactivity of acetone the most and

producing H_2O_2 and CH_3O_2H. These peroxy species can undergo an O-O bond fission yielding OH radicals that are sensitive on the reduction of the IDTs by H-atom abstraction reactions.

4.2.2. JSR experiments

The oxidation of acetone was studied in the JSR at 1.067 bar (800 Torr) for three equivalence ratios (ϕ = 0.5, 1.0 and 2) and an inlet fuel mole fraction of 0.01. The experimental and simulated results are shown in Figure 8. Under the studied conditions, acetone starts to react around 800 K. At ϕ = 1, a conversion rate of 50% is reached at about 950 K and a complete consumption above 1075 K. Compared to pyrolysis (see Figure 3), the presence of oxygen shifts the start of the reactivity by about 82 K, 87 K and 132 K towards lower temperatures for ϕ = 2, 1 and 0.5, respectively. All the products detected in oxidation were also observed in pyrolysis, except for CO_2, which was detected only in oxidation. The formation of benzene is slower under oxidative conditions compared to pyrolysis due to the interaction between benzene precursors, propargyl radicals, and molecular oxygen yielding ketene and formyl radical [71].

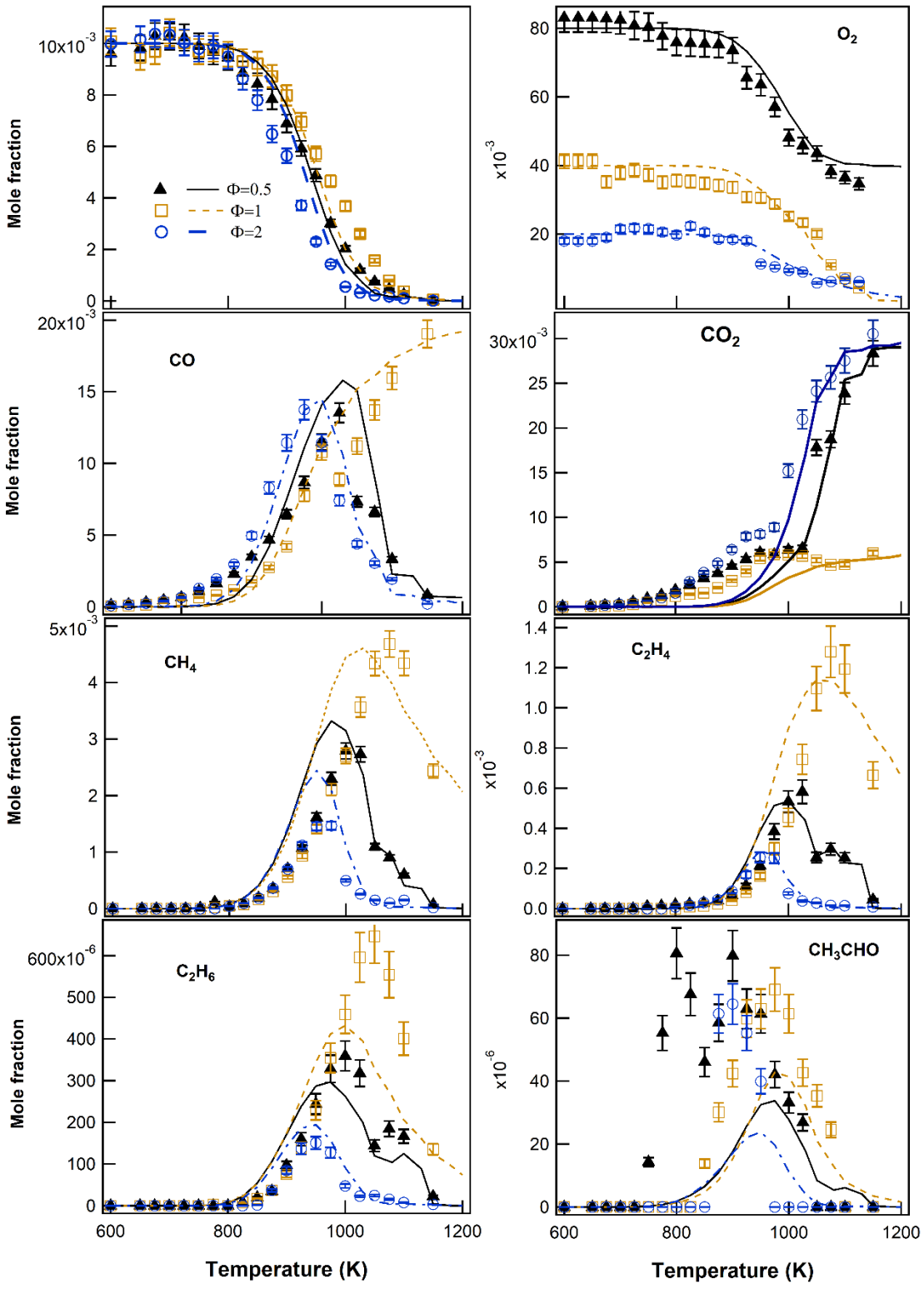

Fig. 8. Mole fraction profiles of the fuel and products during oxidation of acetone in a JSR at ϕ = 0.5, 1 and 2, P = 1.067 bar and τ = 2.0 s. Symbols: experimental data; and lines: computed data.

Deviations between experiments and predictions for acetone conversion can be noted for the three equivalence ratios below 1000 K. The kinetic model predicts the conversion of the fuel at higher temperatures (900 K) than in the experiments, in which fuel consumption is already observed from 800 K. The model does not properly catch the experimental mole fraction profile of CO_2 below 1000 K, where an early formation has been experimentally detected for ϕ = 0.5, 1 and 2, which is consistent with the experimental fuel consumption observed in this temperature range. The drop in CO mole fraction observed around 1000 K at ϕ = 1 might only be due to experimental uncertainty.

The addition of OH on the carbonyl of acetone was theoretically studied [72]. By the reaction $CH_3C(=O)\ CH_3 + OH = CH_3C(=O)\ OH + CH_3$, the formation of acetic acid is expected. However, by adding this reaction to the model, no improvement was observed for the acetic acid mole fraction profiles. Caralp et al. [72] confirmed that the H-atom abstraction reaction from acetone by OH is favored over the addition channel.

Concerning this deviation at low temperature, note that the kinetic model does contain some classic low temperature chemistry (addition of CH_3COCH_2 to O_2 followed by isomerization to CH_2COCH_2OOH radical; the later one reacting by direct decomposition to formaldehyde, ketene and OH, decomposition to a cyclic ether + OH, and second addition to O_2 providing ultimately branching). However, this chemistry does not play a role under the conditions of the present study due to large energy barriers (>48 kcal/mol for the isomerization step [61]). A test was performed to optimize the simulations: a lumped reaction, $CH_3COCH_2 + O_2$, taken from the modeling group in Politecnico di Milano has been included in the model. This reaction leads directly to formaldehyde, ketene and OH with a rate coefficient of 8×10^{11} s^{-1} and no energy barrier [73]. As shown in figure SM2 in SM, the inclusion of this reaction enables to predict the low temperature

reactivity observed in JSR experiments fairly well (example CO_2), but it significantly degrades the agreement for IDTs. Thus, this lumped reaction was not considered in the present kinetic model and the difference in reactivity at low temperature remains unresolved. The undesirable occurrence of heterogeneous reactions at the wall of the reactor cannot be fully excluded. The literature provides several studies about the catalytic oxidation of acetone (e.g., [74,75]) possibly yielding acetaldehyde and carbon dioxide [74], which are the two main reaction products observed in this temperature region. Catalysts are mostly supported ones (e.g., over silica) with metals or metallic oxides as active species. Reactivity onset occurs from 473 K. In the present study, the acetone-O_2 mixture is mainly in contact with fused silica and PFA polymer for which there is no evidence of catalytic activity reported in literature. The only heated metallic parts in contact with the mixture is the sampling loop of the gas chromatograph, but catalytic reactions are very unlikely as the present reactivity onset is observed at a temperature much above that of the sampling loop (and the loop was treated with an inert coating). Important amounts of CO_2 are already observed at low temperature, while those of acetaldehyde remain modest.

Transient behavior has been observed under high-temperature conditions (between 1025-1150 K and at ϕ =1). This transient behavior results in the periodic evolution of the gas phase composition as the function of the time and the steady state cannot be reached. This was previously observed for methane oxidation (Stagni et al. [76]). This phenomenon is typical from oxidation systems rich in methyl radicals. It is a cyclic succession of ignitions and extinctions occurring due to counter-intuitive competitions between pathways the nature, of which depend on the conditions (e.g., equivalence ratio) that cause accumulations of radicals up to a critical radical concentration from which chemical runaway occurs. The reader can refer to [76] for a more detailed analysis of this phenomenon. As described in the experimental method, the time evolution of the species was

measured using a mass spectrometer with online sampling using a capillary tube directly sampling the gas phase in the reactor and by selecting m/z ratio relevant to the species involved in the reaction. Figure 9 displays the time evolution of the mole fraction of the fuel, O_2 and representative products (T = 1050, ϕ = 1).

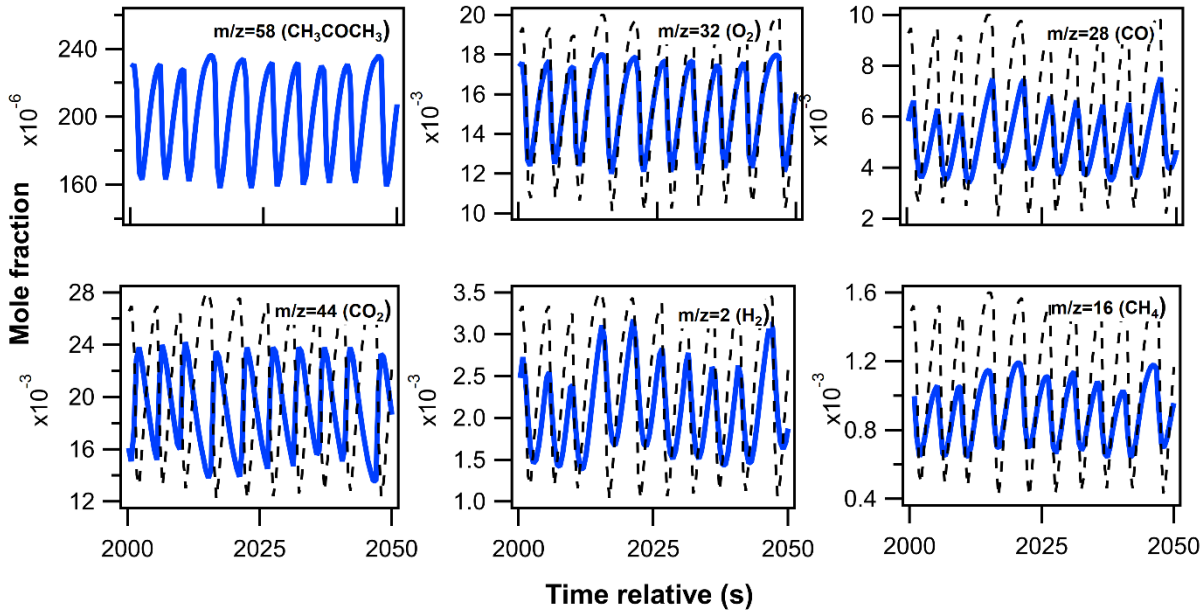

Fig. 9. Experimental mole fraction of acetone, O_2 and representative products recorded for a transient condition (T=1050 K, ϕ = 1) Solid line: mole fraction of the species according to the legend in graphs; dotted line, mole fraction of the fuel (m/z 58) for easier comparison.

When oscillations occur, the mole fractions obtained from GC measurements and presented in Figure 8 are effectively averaged due to injection technique (200 µL sampling loop); the sample is a slice of the reactor outlet flow and the measured mole fraction depends on the sampling loop volume, flow rate, and oscillation properties (frequency, amplitude and periodic shape). Online mass spectrometry provides a better representation of the experimental phenomena when oscillations occur. Figure SM3 presents a comparison of the mole fraction obtained from GC and

those derived from MS data and shows a good consistency between both data sources. Concerning modelling, numerical oscillations were also observed for $\phi = 1$ above 1050 K, as is shown in figure SM-4, which explains the weird simulated traces presented in Figure 8.

The prediction of the mole fraction profile of CO, CH_4 and C_2 compounds are relatively acceptable. While in pyrolysis, the formation of acetaldehyde was overestimated, here it is significantly underestimated.

Figure 10 displays the flow rate for acetone consumption at $\phi = 1$, the analyses at other equivalence ratios are given in Figures SM5 and SM6 in SM. Figures 11 and SM7 in SM present the sensitivity analyses for acetone consumption at $\phi = 1$ and 2 and at $\phi = 0.5$, respectively. Under rich conditions, no sensitivity is found for reactions directly deriving from acetone.

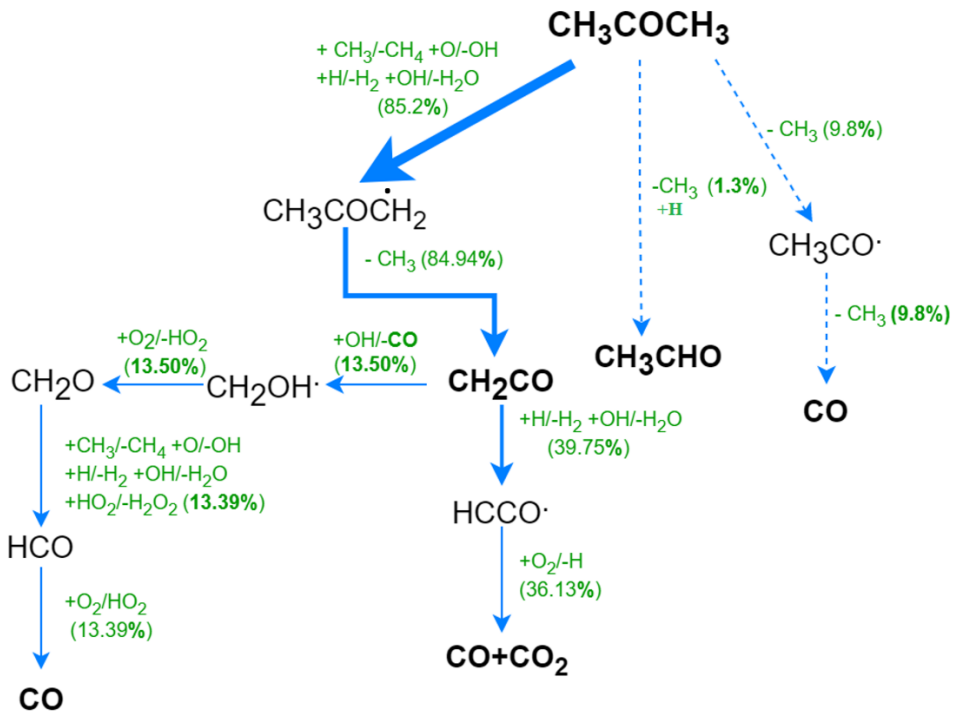

Fig. 10. The reaction pathway network in the JSR oxidation of acetone at $\phi = 1$. Conditions of simulation: 1000 K, 1.067 bar, residence time of 2 s corresponding to 50 % conversion.

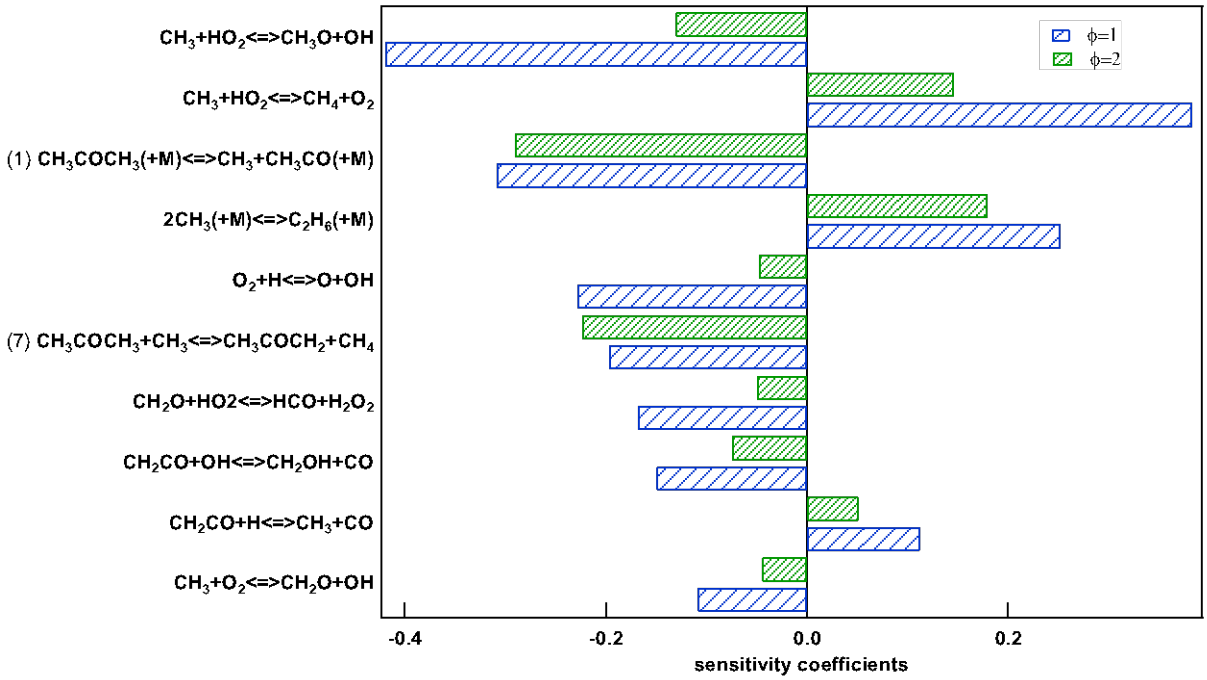

Fig. 11. Sensitive reactions to the mole fraction of acetone during oxidation at ϕ = 1 and 2 at 1000 K.

For the three equivalence ratios, the major consumption pathways of acetone are similar with a major production of CH_3COCH_2 radical by H-abstractions. This radical is then mainly consumed by reaction R14 to produce ketene (CH_2CO) and CH_3 radicals. Ketene is mainly consumed by OH-addition to produce CH_2OH yielding formaldehyde and by H-abstractions to yield HCCO, a source of CO and CO_2. As shown in Figure 11, under stoichiometric conditions, the reaction $CH_3+HO_2<=>CH_3O+OH$ has the highest promoting effect for acetone consumption. Conversely, the competing reaction, $CH_3+HO_2<=>CH_4+O_2$, has the largest inhibiting effect at ϕ =1 and 2, while it has a promoting effect at ϕ =0.5. The recombination of two CH_3 radicals plays an inhibiting role for acetone consumption, as it is one of the termination steps in the pyrolysis process for the three equivalence ratios. Note also the significant promoting effect of acetone unimolecular decomposition, CH_3COCH_3 (+M) <=> CH_3+CH_3CO (+M). This kinetic analysis shows that the

methyl radical is playing a crucial role under these “high” temperature conditions. Note that this radical is also involved in the oscillation behavior observed for specific temperature and equivalence ratio conditions. Nevertheless, a direct parallel cannot be made between the situation in Figure 11 and that displayed in Figure 9 (oscillations) as conditions are different and as the data in Figure 11 are for a condition where steady state is obtained.

As an intermediate conclusion, under pyrolytic conditions in a JSR, the consumption of acetone is initiated by the unimolecular decomposition reaction. It forms a methyl radical that can abstract an H-atom from the fuel and lead to the acetonyl radical. This radical undergoes a β-scission that forms again a methyl radical. Overall, CH_3 leads the pyrolysis of acetone.

To the contrary of pyrolysis, the unimolecular decomposition is a minor pathway in the oxidation process of acetone. Here, the H-atom abstraction reactions by OH and CH_3 radicals are important pathways of reaction. However, the sensitivity analysis (fig. 11) shows that the most sensitive reactions during the oxidation of acetone are relative to the methyl radical. The fate of this radical dictates the overall oxidation behavior of acetone. $CH_3 + HO_2 = CH_4 + O_2$ or the recombination $CH_3 + CH_3 (+M) = C_2H_6 (+M)$ depletes the radical pool while $CH_3 + HO_2 = CH_2O + OH$ or $CH_3 + O_2 = CH_2O + OH$ forms the OH radical.

To summarize, under the studied conditions in a JSR, the combustion of acetone occurs via the formation of the methyl radical and an accurate submechanism of the combustion of methane is required to obtain precise simulations.

Now concerning the behavior of acetaldehyde: In absence of oxygen, the H-atom addition on the carbonyl seems a legit pathway of production of acetaldehyde. The reaction rate used in this study

could be refined to match with the experimental data (reaction 13 in table 2). Nevertheless, we preferred to use the rate calculated by Thion et al. for butanone [52].

In oxidative conditions, the effect of the aforementioned addition is not sufficient to explain the observed mole fraction of acetaldehyde. From figure 8, we can observe that the quantities of acetaldehyde formed does not vary with equivalence ratio. It eliminates the hypothesis of the involvement of an oxygenated radical in the CH_3CHO production process. However, no convincing reaction pathway was found and we believe that this matter could benefit from further work.

4.2.3. Burning velocity measurements

Adiabatic laminar burning velocity measurements were performed under atmospheric pressure. The vapor pressure of acetone is high enough to allow experiments at several fresh gas temperatures: 306, 358 and 398 K. The ranges of investigated equivalence ratios are limited by flame instabilities or extinction under lean and rich conditions. For each temperature, the experiments are performed over larger equivalence ratio ranges than previous studies in the literature. Numerical data is calculated using the Premixed Laminar Flame-Speed module in Chemkin Pro software. The Soret effect is considered and the numerical parameters GRAD and CURV are both equal to 0.1.

At 1 bar, while a lot of measurements were performed at ambient temperature [21,24–26,29,32–34], only Nilsson et al. [25] completed experiments at 358 K and 3 studies exist with data around 398 K [27,28,31]. Other works were achieved under other conditions (see Table 1). As shown in Figure 12a, at ambient temperature, the results are in good agreement with those of Nilsson and al. [25] and Chong et al. [29] under lean conditions. They are also in good agreement with those of Konnov et al. [24] for rich mixtures. The results obtained with the bomb method [21,26,34] are

scattered; for lean compositions, they all are lower than in that work. Data obtained with the heat flux method (Nilsson et al. [25], Konnov et al. [24] and this work) are in good agreement, in particular for rich mixtures. At 358 K (Figure 12b), there is a good agreement between our results and Nilsson's ones except at ϕ =0.6. At 398 K (Figure 13c), the current experimental data are between the other sets of measurements; all results are extremely close under rich conditions. Figure SM8 in SM plot all the investigated temperature on the same graph. In each case the predictions fit relatively well the experimental data. However the kinetic model slightly overestimates the current burning velocity results around ϕ =1.1.

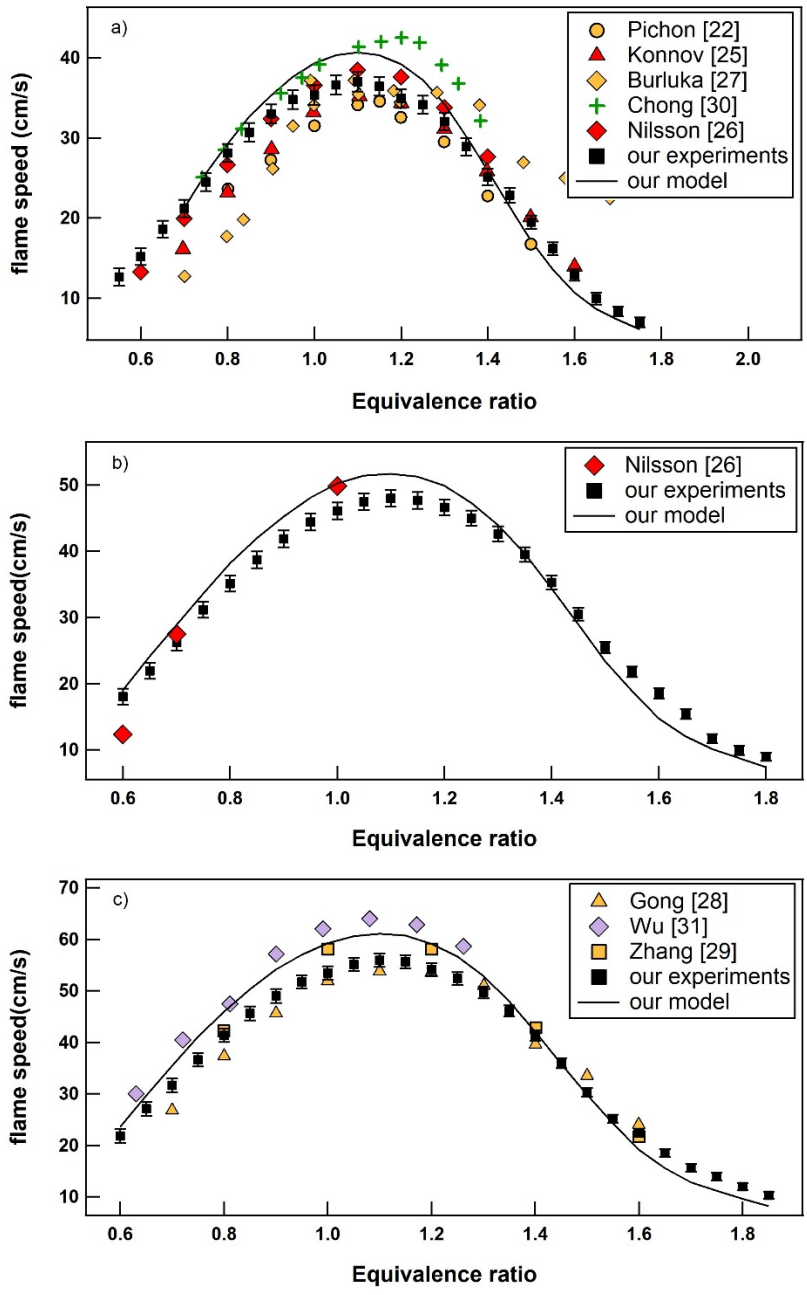

Fig. 12. Adiabatic laminar flame velocities of acetone in air under atmospheric pressure. a) 306 K *(Numerical calculations don't converge under ϕ =0.65)*, b) 358 K and c) 398 K.

5. Conclusion

In this work, IDTs were measured at pressures of 20 and 40 bar and temperatures from 850 to 1100 K. Experiments in a JSR coupled with GC were performed for pyrolysis (700-1200 K) and for oxidation (600-1150 K), with the quantified products being methane, ethane, and ethylene in both cases, with also acetaldehyde, CO and CO_2 for oxidation. A detailed investigation of the observed transient behavior above 1000 K was also made. In addition, laminar burning velocities were measured at various fresh gas temperature (ambient temperature, 358 K and 398 K). Overall laminar burning velocities agree with the existing values from the literature and in particular those obtained with a similar device. However, the literature experimental data are somehow scattered which could seem surprising for such a small fuel. A new detailed kinetic model of acetone has been developed in this work and allows to reproduce reasonably well the experimental data obtained. This is especially the case for the fuel reactivity and the mole fraction of major intermediates, except for CO_2 in oxidation below 1000 K. Deviations were observed for some minor species produced like acetaldehyde. Better predictions would likely benefit from revisiting the chemistry of formation and consumption of this small aldehyde which is a common intermediate in many oxidation studies.

6. Acknowledgement

The Nancy work has received funding from the European Union's Horizon 2020 research and innovation program (BUILDING A LOW-CARBON, CLIMATE RESILIENT FUTURE: SECURE, CLEAN AND EFFICIENT ENERGY) under Grant Agreement No 101006744. The content presented in this document represents the views of the authors, and the European Commission has no liability in respect of the content. In Aachen, this work was performed as part of the Cluster of Excellence "The Fuel Science Center" and funded by the Deutsche Forschungsgemeinschaft (DFG, German Research Foundation) under Germany´s Excellence Strategy – Cluster of Excellence 2186 – ID: 390919832

7. Reference

[1] Z. Liu, F.-S. Zhang, Effects of various solvents on the liquefaction of biomass to produce fuels and chemical feedstocks, Energ. Convers. Manage. 49 (2008) 3498–3504. https://doi.org/10.1016/j.enconman.2008.08.009.

[2] Y. Li, K. Nithyanandan, X. Meng, T.H. Lee, Y. Li, C.F. Lee, Z. Ning, Experimental study on combustion and emission performance of a spark-ignition engine fueled with water containing acetone-gasoline blends, Fuel. 210 (2017) 133–144. https://doi.org/10.1016/j.fuel.2017.07.058.

[3] A. Elfasakhany, Investigations on performance and pollutant emissions of spark-ignition engines fueled with n-butanol–, isobutanol–, ethanol–, methanol–, and acetone–gasoline blends: A comparative study, Renew. Sust. Energ. Rev. 71 (2017) 404–413. https://doi.org/10.1016/j.rser.2016.12.070.

[4] L. Meng, C. Zeng, Y. Li, K. Nithyanandan, T.H. Lee, C. Lee, An Experimental Study on the Potential Usage of Acetone as an Oxygenate Additive in PFI SI Engines, Energies. 9 (2016) 256. https://doi.org/10.3390/en9040256.

[5] M. Tymchyshyn, A. Rezayan, Z. Yuan, Y. Zhang, C.C. Xu, Reductive Hydroprocessing of Hydrolysis Lignin over Efficient Bimetallic Catalyst MoRu/AC, Ind. Eng. Chem. Res. 59 (2020) 17239–17249. https://doi.org/10.1021/acs.iecr.0c01151.

[6] B. Yip, M.F. Miller, A. Lozano, R.K. Hanson, A combined OH/acetone planar laser-induced fluorescence imaging technique for visualizing combusting flows, Exp. Fluids. 17 (1994) 330–336. https://doi.org/10.1007/BF01874413.

[7] H. Singh, Y. Chen, A. Staudt, D. Jacob, D. Blake, B. Heikes, J. Snow, Evidence from the Pacific troposphere for large global sources of oxygenated organic compounds, Nature. 410 (2001) 1078–1081. https://doi.org/10.1038/35074067.

[8] M.A.H. Khan, M.C. Cooke, S.R. Utembe, A.T. Archibald, P. Maxwell, W.C. Morris, P. Xiao, R.G. Derwent, M.E. Jenkin, C.J. Percival, R.C. Walsh, T.D.S. Young, P.G. Simmonds, G. Nickless, S. O'Doherty, D.E. Shallcross, A study of global atmospheric budget and distribution of acetone using global atmospheric model STOCHEM-CRI, Atmos. Environ. 112 (2015) 269–277. https://doi.org/10.1016/j.atmosenv.2015.04.056.

[9] M. Szewczyńska, E. Dobrzyńska, M. Pośniak, Qualitative analysis of highly toxic organic compunds emitted from uncontrolled combustion sources using GC-MS/MS, Anal. Chem. 53 (2008) 59–70.

[10] D.J. Jacob, B.D. Field, E.M. Jin, I. Bey, Q. Li, J.A. Logan, R.M. Yantosca, H.B. Singh, Atmospheric budget of acetone, J. Geophys. Res-Atmos. 107 (2002) ACH 5-1-ACH 5-17. https://doi.org/10.1029/2001JD000694.

[11] B.C. Capelin, G. Ingram, J. Kokolis, The pyrolytic identification of organic molecules: II. A quantitative evaluation, Microchem. J. 19 (1974) 229–252. https://doi.org/10.1016/0026-265X(74)90123-4.

[12] J. Ernst, K. Spindler, H.G. Wagner, Untersuchungen zum thermischen Zerfall von Acetaldehyd und Aceton, Berich. Bunsen Gesell. 80 (1976) 645–650. https://doi.org/10.1002/bbpc.19760800713.

[13] K. Sato, Y. Hidaka, Shock-tube and modeling study of acetone pyrolysis and oxidation, Combust. Flame. 122 (2000) 291–311. https://doi.org/10.1016/S0010-2180(00)00121-8.

[14] D. Yu, Z.-Y. Tian, Z. Wang, Y.-X. Liu, L. Zhou, Experimental and theoretical study on acetone pyrolysis in a jet-stirred reactor, Fuel. 234 (2018) 1380–1387.

[15] D.P. Zaleski, R. Sivaramakrishnan, H.R. Weller, N.A. Seifert, D.H. Bross, B. Ruscic, K.B. Moore, S.N. Elliott, A.V. Copan, L.B. Harding, S.J. Klippenstein, R.W. Field, K. Prozument, Substitution Reactions in the Pyrolysis of Acetone Revealed through a Modeling, Experiment, Theory Paradigm, J. Am. Chem. Soc. 143 (2021) 3124–3142. https://doi.org/10.1021/jacs.0c11677.

[16] J.A. Barnard, T.W. Honeyman, The Gaseous Oxidation of Acetone. I. The High-Temperature Reaction, P. R. Soc. Lond. A-Conta. 279 (1964) 236–247. https://doi.org/10.1098/rspa.1964.0101.
[17] J.A. Barnard, T.W. Honeyman, The Gaseous Oxidation of Acetone. II. The Low-Temperature Reaction, P. R. Soc. Lond. A-Conta. 279 (1964) 248–259. https://doi.org/10.1098/rspa.1964.0102.
[18] D.E. Hoare, T.-M. Li, The combustion of simple ketones I— Mechanism at 'low' temperatures, Combust. Flame. 12 (1968) 136–144. https://doi.org/10.1016/0010-2180(68)90089-8.
[19] D.E. Hoare, D.E. Lill, Branching intermediates in the cool flames of acetaldehyde and simple ketones, J. Chem. Soc. Farad. T. 1. 69 (1973) 603–613. https://doi.org/10.1039/F19736900603.
[20] T. Tsuboi, K. Ishii, S. Tamura, Thermal oxidation of acetone behind reflected shock wave, (n.d.) 4.
[21] S. Pichon, G. Black, N. Chaumeix, M. Yahyaoui, J.M. Simmie, H.J. Curran, R. Donohue, The combustion chemistry of a fuel tracer: Measured flame speeds and ignition delays and a detailed chemical kinetic model for the oxidation of acetone, Combust. Flame. 156 (2009) 494–504. https://doi.org/10.1016/j.combustflame.2008.10.001.
[22] Y. Li, L. Wei, Z. Tian, B. Yang, J. Wang, T. Zhang, F. Qi, A comprehensive experimental study of low-pressure premixed C3-oxygenated hydrocarbon flames with tunable synchrotron photoionization, Combust. Flame. 152 (2008) 336–359. https://doi.org/10.1016/j.combustflame.2007.10.012.
[23] H. Liao, T. Tao, W. Sun, N. Hansen, B. Yang, Isomer-specific speciation behaviors probed from premixed flames fueled by acetone and propanal, P. Combust. Inst. 38 (2021) 2441–2448. https://doi.org/10.1016/j.proci.2020.06.221.
[24] A.A. Konnov, R.J. Meuwissen, L.P.H. de Goey, Laminar burning velocities of acetone + air flames at room and elevated temperatures, (2009).
[25] E.J.K. Nilsson, L.P.H. de Goey, A.A. Konnov, Laminar burning velocities of acetone in air at room and elevated temperatures, Fuel. 105 (2013) 496–502. https://doi.org/10.1016/j.fuel.2012.07.047.
[26] A.A. Burluka, M. Harker, H. Osman, C.G.W. Sheppard, A.A. Konnov, Laminar burning velocities of three C3H6O isomers at atmospheric pressure, Fuel. 89 (2010) 2864–2872. https://doi.org/10.1016/j.fuel.2010.02.004.
[27] J. Gong, S. Zhang, Y. Cheng, Z. Huang, C. Tang, J. Zhang, A comparative study of n -propanol, propanal, acetone, and propane combustion in laminar flames, P. Combust. Inst. 35 (2015) 795–801. https://doi.org/10.1016/j.proci.2014.05.066.
[28] S. Zhang, T.H. Lee, H. Wu, J. Pei, W. Wu, F. Liu, Experimental and Kinetical Study of Component Volumetric Effects on Laminar Flame Speed of Acetone–Butanol–Ethanol (ABE), Energ. Fuel. 32 (2018) 6278–6292. https://doi.org/10.1021/acs.energyfuels.8b00003.
[29] C.T. Chong, S. Hochgreb, Measurements of laminar flame speeds of acetone/methane/air mixtures, Combust. Flame. 158 (2011) 490–500. https://doi.org/10.1016/j.combustflame.2010.09.019.
[30] Y. Wu, V. Modica, B. Rossow, F. Grisch, Effects of pressure and preheating temperature on the laminar flame speed of methane/air and acetone/air mixtures, Fuel. 185 (2016) 577–588. https://doi.org/10.1016/j.fuel.2016.07.110.
[31] Y. Wu, V. Modica, X. Yu, F. Li, F. Grisch, Effects of optical diagnostic techniques on the accuracy of laminar flame speeds measured from Bunsen flames: OH\ast chemiluminescence, OH-PLIF and acetone/kerosene-PLIF, Meas. Sci. Technol. 29 (2017) 1–11. https://doi.org/10.1088/1361-6501/aa92d7.
[32] G.J. Gibbs, H.F. Calcote, Effect of Molecular Structure on Burning Velocity., J. Chem. Eng. Data. 4 (1959) 226–237. https://doi.org/10.1021/je60003a011.
[33] L.N. Khitrin, The physics of combustion and explosion. (Fizika goreniya i vzryva), Israel Program for Scientific Translations, Jerusalem, 1962.
[34] V.V. Mol'kov, V.P. Nekrasov, Normal propagation velocity of acetone-air flames versus pressure and temperature, Combust. Explo. Shock+. 17 (1981) 280–283. https://doi.org/10.1007/BF00751300.

[35] K.J. Bosschaart, L.P.H. de Goey, The laminar burning velocity of flames propagating in mixtures of hydrocarbons and air measured with the heat flux method, Combust. Flame. 136 (2004) 261–269. https://doi.org/10.1016/j.combustflame.2003.10.005.
[36] O. Herbinet, B. Husson, H. Le Gall, F. Battin-Leclerc, An experimental and modeling study of the oxidation of n-heptane, ethylbenzene, and n-butylbenzene in a jet-stirred reactor at pressures up to 10 bar, Int. J. Chem. Kinet. 52 (2020) 1006–1021. https://doi.org/10.1002/kin.21417.
[37] S. Namysl, M. Pelucchi, L. Pratali Maffei, O. Herbinet, A. Stagni, T. Faravelli, F. Battin-Leclerc, Experimental and modeling study of benzaldehyde oxidation, Combust. Flame. 211 (2020) 124–132. https://doi.org/10.1016/j.combustflame.2019.09.024.
[38] M. Pelucchi, S. Arunthanayothin, Y. Song, O. Herbinet, A. Stagni, H.-H. Carstensen, T. Faravelli, F. Battin-Leclerc, Pyrolysis and Combustion Chemistry of Pyrrole, a Reference Component for Bio-oil Surrogates: Jet-Stirred Reactor Experiments and Kinetic Modeling, Energ. Fuel. 35 (2021) 7265–7284. https://doi.org/10.1021/acs.energyfuels.0c03874.
[39] R.J. Kee, F.M. Rupley, J.A. Miller, M.E. Coltrin, J.F. Grcar, E. Meeks, H.K. Moffat, A.E. Lutz, G. Dixon-Lewis, M.D. Smooke, CHEMKIN collection, release 3.6, reaction design, Inc., San Diego, CA. 20 (2000) 0.
[40] O. Herbinet, Etude expérimentale et modélisation de la décomposition thermique de l'exo-tricyclo [5.2.1.0 2,6] décane, Theses, Institut National Polytechnique de Lorraine, 2006. https://hal.univ-lorraine.fr/tel-01752479 (accessed February 10, 2022).
[41] M. Lubrano Lavadera, Y. Song, P. Sabia, O. Herbinet, M. Pelucchi, A. Stagni, T. Faravelli, F. Battin-Leclerc, M. de Joannon, Oscillatory Behavior in Methane Combustion: Influence of the Operating Parameters, Energ. Fuel. 32 (2018) 10088–10099. https://doi.org/10.1021/acs.energyfuels.8b00967.
[42] C. Lee, S. Vranckx, K.A. Heufer, S.V. Khomik, Y. Uygun, H. Olivier, R.X. Fernandez, On the Chemical Kinetics of Ethanol Oxidation: Shock Tube, Rapid Compression Machine and Detailed Modeling Study, Z. Phys. Chem. 226 (2012) 1–28. https://doi.org/10.1524/zpch.2012.0185.
[43] A. Ramalingam, K. Zhang, A. Dhongde, L. Virnich, H. Sankhla, H. Curran, A. Heufer, An RCM experimental and modeling study on CH4 and CH4/C2H6 oxidation at pressures up to 160bar, Fuel. 206 (2017) 325–333. https://doi.org/10.1016/j.fuel.2017.06.005.
[44] Gaseq Chemical Equilibrium Program, (n.d.). http://www.gaseq.co.uk/ (accessed August 20, 2021).
[45] S.S. Goldsborough, S. Hochgreb, G. Vanhove, M.S. Wooldridge, H.J. Curran, C.-J. Sung, Advances in rapid compression machine studies of low- and intermediate-temperature autoignition phenomena, Prog. Energ. Combust. 63 (2017) 1–78. https://doi.org/10.1016/j.pecs.2017.05.002.
[46] C.-J. Sung, H.J. Curran, Using rapid compression machines for chemical kinetics studies, Prog. Energ. Combust. 44 (2014) 1–18. https://doi.org/10.1016/j.pecs.2014.04.001.
[47] P. Dirrenberger, P.A. Glaude, R. Bounaceur, H. Le Gall, A.P. da Cruz, A.A. Konnov, F. Battin-Leclerc, Laminar burning velocity of gasolines with addition of ethanol, Fuel. 115 (2014) 162–169. https://doi.org/10.1016/j.fuel.2013.07.015.
[48] L.-S. Tran, M. Verdicchio, F. Monge, R.C. Martin, R. Bounaceeur, B. Sirjean, P.-A. Glaude, M.U. Alzueta, F. Battin-Leclerc, An experimental and modeling study of the combustion of tetrahydrofuran, Combust. Flame. 162 (2015) 1899–1918. https://doi.org/10.1016/j.combustflame.2014.12.010.
[49] C.-W. Zhou, Y. Li, U. Burke, C. Banyon, K.P. Somers, S. Ding, S. Khan, J.W. Hargis, T. Sikes, O. Mathieu, E.L. Petersen, M. AlAbbad, A. Farooq, Y. Pan, Y. Zhang, Z. Huang, J. Lopez, Z. Loparo, S.S. Vasu, H.J. Curran, An experimental and chemical kinetic modeling study of 1,3-butadiene combustion: Ignition delay time and laminar flame speed measurements, Combust. Flame. 197 (2018) 423–438. https://doi.org/10.1016/j.combustflame.2018.08.006.
[50] Y. Fenard, J. Pieper, C. Hemken, H. Minwegen, R.D. Büttgen, K. Kohse-Höinghaus, K.A. Heufer, Experimental and modeling study of the low to high temperature oxidation of the linear pentanone

isomers: 2-pentanone and 3-pentanone, Combust. Flame. 216 (2020) 29–44. https://doi.org/10.1016/j.combustflame.2020.02.015.
[51] H.J. Curran, P. Gaffuri, W.J. Pitz, C.K. Westbrook, A Comprehensive Modeling Study of n-Heptane Oxidation, Combust. Flame. 114 (1998) 149–177. https://doi.org/10.1016/S0010-2180(97)00282-4.
[52] S. Thion, P. Diévart, P. Van Cauwenberghe, G. Dayma, Z. Serinyel, P. Dagaut, An experimental study in a jet-stirred reactor and a comprehensive kinetic mechanism for the oxidation of methyl ethyl ketone, P. Combust. Inst. 36 (2017) 459–467. https://doi.org/10.1016/j.proci.2016.05.022.
[53] S. Saxena, J.H. Kiefer, S.J. Klippenstein, A shock-tube and theory study of the dissociation of acetone and subsequent recombination of methyl radicals, P. Combust. Inst. 32 (2009) 123–130. https://doi.org/10.1016/j.proci.2008.05.032.
[54] S.J. Klippenstein, Y. Georgievskii, L.B. Harding, Predictive theory for the combination kinetics of two alkyl radicals, Phys. Chem. Chem. Phys. (2006) 8, 1133-1147. https://doi-org/10.1039/B515914H.
[55] V. Saheb, M. Zokaie, Multichannel Gas-Phase Unimolecular Decomposition of Acetone: Theoretical Kinetic Studies, J. Phys. Chem. A. 122 (2018) 5895–5904. https://doi.org/10.1021/acs.jpca.8b02423.
[56] K.-Y. Lam, W. Ren, S.H. Pyun, A. Farooq, D.F. Davidson, R.K. Hanson, Multi-species time-history measurements during high-temperature acetone and 2-butanone pyrolysis, P. Combust. Inst. 34 (2013) 607–615. https://doi.org/10.1016/j.proci.2012.06.009.
[57] D. Yu, Z.-Y. Tian, Z. Wang, Y.-X. Liu, L. Zhou, Experimental and theoretical study on acetone pyrolysis in a jet-stirred reactor, Fuel. 234 (2018) 1380–1387.
[58] C.-W. Zhou, J.M. Simmie, H.J. Curran, Ab initio and kinetic study of the reaction of ketones with ȮH for T = 500–2000 K. Part I: hydrogen-abstraction from H3CC(O)CH3–x(CH3)x, x = 0 ↦ 2, Phys. Chem. Chem. Phys. 13 (2011) 11175–11192. https://doi.org/10.1039/C0CP02754E.
[59] J. Mendes, C.-W. Zhou, H.J. Curran, Theoretical and Kinetic Study of the Reactions of Ketones with HȮ2 Radicals. Part I: Abstraction Reaction Channels, J. Phys. Chem. A. 117 (2013) 4515–4525. https://doi.org/10.1021/jp4000413.
[60] W.A. Kopp, U. Burke, M. Döntgen, L.C. Kröger, H. Minwegen, K.A. Heufer, K. Leonhard, Ab initio kinetics predictions for H-atom abstraction from 2-butanone by Ḣ and Ċ H3 and the subsequent unimolecular reactions, P. Combust. Inst. 36 (2017) 203–210. https://doi.org/10.1016/j.proci.2016.06.162.
[61] P.R. Parab, K.A. Heufer, R.X.F. Fernandes, Computational Chemical Kinetics of Biofuel Combustion Using Ab-Initio Methods and Statistical Rate Theories, Shaker, 2018. https://publications.rwth-aachen.de/record/712123 (accessed July 7, 2021).
[62] J. Bugler, K.P. Somers, E.J. Silke, H.J. Curran, Revisiting the Kinetics and Thermodynamics of the Low-Temperature Oxidation Pathways of Alkanes: A Case Study of the Three Pentane Isomers, J. Phys. Chem. A. 119 (2015) 7510–7527. https://doi.org/10.1021/acs.jpca.5b00837.
[63] M. Keiffer, A.J. Miscampbell, M.J. Pilling, A global technique for analysing multiple decay curves. Application to the CH3+ O2 system, J. Chem. Soc. Farad. T. 2. 84 (1988) 505–514. https://doi.org/10.1039/F29888400505.
[64] C. Hemken, U. Burke, K.-Y. Lam, D.F. Davidson, R.K. Hanson, K.A. Heufer, K. Kohse-Höinghaus, Toward a better understanding of 2-butanone oxidation: Detailed species measurements and kinetic modeling, Combust. Flame. 184 (2017) 195–207. https://doi.org/10.1016/j.combustflame.2017.06.007.
[65] J. Badra, A.E. Elwardany, F. Khaled, S.S. Vasu, A. Farooq, A shock tube and laser absorption study of ignition delay times and OH reaction rates of ketones: 2-Butanone and 3-buten-2-one, Combust. Flame. 161 (2014) 725–734. https://doi.org/10.1016/j.combustflame.2013.10.001.
[66] U. Burke, J. Beeckmann, W.A. Kopp, Y. Uygun, H. Olivier, K. Leonhard, H. Pitsch, K.A. Heufer, A comprehensive experimental and kinetic modeling study of butanone, Combust. Flame. 168 (2016) 296–309. https://doi.org/10.1016/j.combustflame.2016.03.001.

[67] R.D. Büttgen, M. Tian, Y. Fenard, H. Minwegen, M.D. Boot, K.A. Heufer, An experimental, theoretical and kinetic modelling study on the reactivity of a lignin model compound anisole under engine-relevant conditions, Fuel. 269 (2020) 117190. https://doi.org/10.1016/j.fuel.2020.117190.
[68] C.W. Gao, J.W. Allen, W.H. Green, R.H. West, Reaction Mechanism Generator: Automatic construction of chemical kinetic mechanisms, Computer Physics Communications. 203 (2016) 212–225. https://doi.org/10.1016/j.cpc.2016.02.013.
[69] J.A. Miller, S.J. Klippenstein, The Recombination of Propargyl Radicals and Other Reactions on a C_6H_6 Potential, J. Phys. Chem. A. 107 (2003) 7783–7799. https://doi.org/10.1021/jp030375h.
[70] J.A. Miller, M.J. Pilling, J. Troe, Unravelling combustion mechanisms through a quantitative understanding of elementary reactions, P. Combust. Inst. 30 (2005) 43–88. https://doi.org/10.1016/j.proci.2004.08.281.
[71] D.K. Hahn, S.J. Klippenstein, J.A. Miller, A theoretical analysis of the reaction between propargyl and molecular oxygen, Faraday Discuss. 119 (2002) 79–100. https://doi.org/10.1039/B102240G.
[72] F. Caralp, W. Forst, E. Hénon, A. Bergeat, F. Bohr, Tunneling in the reaction of acetone with OH, Phys. Chem. Chem. Phys. 8 (2006) 1072. https://doi.org/10.1039/b515118j.
[73] G. Bagheri, E. Ranzi, M. Pelucchi, A. Parente, A. Frassoldati, T. Faravelli, Comprehensive kinetic study of combustion technologies for low environmental impact: MILD and OXY-fuel combustion of methane, Combust. Flame. 212 (2020) 142–155. https://doi.org/10.1016/j.combustflame.2019.10.014.
[74] M. Baldi, E. Finocchio, F. Milella, G. Busca, Catalytic combustion of C3 hydrocarbons and oxygenates over Mn3O4, Applied Catalysis B: Environmental. 16 (1998) 43–51. https://doi.org/10.1016/S0926-3373(97)00061-1.
[75] F. Rachedi, R. Guilet, P. Cognet, J. Tasselli, A. Marty, P. Dubreuil, Microreactor for Acetone Deep Oxidation over Platinum, Chem. Eng. Technol. 32 (2009) 1766–1773. https://doi.org/10.1002/ceat.200900378.
[76] A. Stagni, Y. Song, L.A. Vandewalle, K.M. Van Geem, G.B. Marin, O. Herbinet, F. Battin-Leclerc, T. Faravelli, The role of chemistry in the oscillating combustion of hydrocarbons: An experimental and theoretical study, Chem. Eng. J. 385 (2020) 123401. https://doi.org/10.1016/j.cej.2019.123401.